Hydrogen, anti-hydrogen beams production in a long linear vacuum pipe

(submited to Nucl. Inst. Meth.)

André Rosowsky[a]

[a]CEA-CE Saclay-DSM/DAPNIA/SPP, 91191 Gif-sur-Yvette, France

This paper presents the possible production of hydrogen and anti-hydrogen from $p^{\pm}$and $e^{\mp}$beams merged in a long vacuum chamber (about 2500 m). In such a configuration with a beam kinetic energy for the $p^{\pm}$around 100 KeV, the two key parameters are the density of the $e^{\mp}$beam and the temperature of the merged beams. The production rate is computed for several parameter sets and it is shown that it is possible to recombine $10^6 p^{\pm}$ with nearly 100% efficiency. Possible experiments using this configuration are presented, including the fine structure constant measurement, the anti-hydrogen spectroscopy and the comparison of the gravitational mass for hydrogen and antihydrogen. PACS numbers: 25.43.+t (antiproton and antihydrogen), 06.20.Jr (fine structure constant, gravitational mass), 41.75.Lx (crystalline beams)

1. Introduction

Several experiments using storage rings or electromagnetic traps have been proposed to produce and store anti-hydrogen [2,19]. In both cases it is expected that the anti-hydrogen atoms are produced at very low rates. The configuration proposed here is a long vacuum pipe inside which the particles travel only once and the anti-hydrogen is produced by bursts of about 10^6 atoms. The topics presented and discussed are the following:

- the configuration and the different sets of beam hypothesis,
- the computation of the production rate and its application to the different sets,
- the focussing of the anti-atom or atom beam at the exit of the pipe,
- the experiments'configurations.

In the last section the production of p^- is briefly discussed. The hydrogen atom is referred to as H while the anti-hydrogen atom is referred to as $\tilde{H}$.

2. Configuration and hypotheses

The general set-up is shown in figure 1. It is derived from the existing experiments made at ion storage rings where ion beams are merged with electrons in an electron cooler [5]. The recombination region defined by the length of the cooler is approximatively 1 meter and the unused ions are recycled in the storage ring and re-used at the next path through the cooler. In the long pipe configuration, the ions are not recycled but the interaction time, defined by the duration of the two beams superposition, is about 2500 larger. This longer time allows for a recombination of all the p^- up to 10^6 particles (see section 4). The point where the beams are injected will be referred to as the *entry* and the other pipe extremity as the *exit*.

The other features of ion storage ring experiments are identical here: the $e^{\mp}$beam has a diameter of approximatively $1 \sim 2\,cm$ and the cooled $p^{\pm}$beam collapses into a cylinder of approximatively 2 mm. The $e^{\mp}$beam is kept within this diameter along the 2500 m by a weak magnetic field.

As the experiments on the radiative recombination into hydrogen atoms of $e^- p^+$ have shown, the reaction can be enhanced by a laser [4,5]. Both cases, with and without laser induced radiative recombination, will be considered. When there is a laser, the light is injected from the exit of the pipe. The photon energy seen in the rest frame of the $p^{\pm}$is then Doppler shifted.

The atom production rate is computed for several sets of parameters, including some very dif-

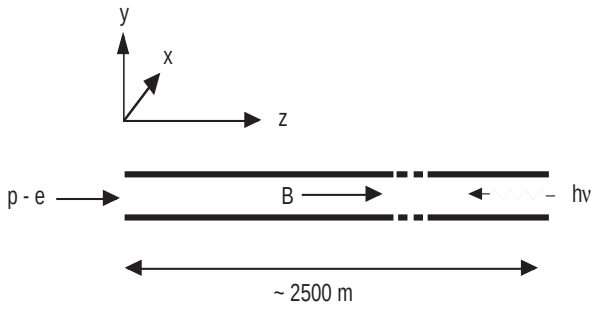

Figure 1. Merged beams configuration: the two beams are injected and superposed on one side and the laser light is injected at the other side. A weak magnetic field parallel to the pipe is used to guide the $e^{\mp}$ beam.

ferent from the suggested ones: these sets have been chosen to compare the results with past experiments. Each set contains:

- the kinetic energy of the $p^{\pm}$: $K(p^{\pm})$,
- the corresponding kinetic energy for the $e^{\mp}$ to have the same velocity: $K(e^{\mp})$,
- the velocity: V,
- the relativistic coefficients: β,γ,
- the time of flight across the pipe: τ,
- the Doppler factor: $\sqrt{\frac{1+\beta}{1-\beta}}$.

Tables 1 and 2 correspond to a long time of flight in order to produce beams of $10^5 \sim 10^6$ $\tilde{H}$ per burst.

Table 3 corresponds to the kinetic energy of the p^- beam produced at CERN with the Antiproton Decelerator (AD). Table 4 shows the kinetic energy required to have a Doppler shift factor of 5 suited for the boosted spectroscopy experiment to be presented in a later section.

The experiments on the radiative recombination of $e^- p^+$ into hydrogen atoms performed at

Table 1
Set 1

$p^{\pm}$	$50 \quad KeV$
$e^{\mp}$	$27.23085 \quad eV$
γ	1.00005328943
β	0.0103232912
V	$3094844.8551\, m.s^{-1}$
τ	$0.808\, 10^{-3} \quad s$
$\sqrt{\frac{1+\beta}{1-\beta}}$	1.01037713079

Table 2
Set 2 represent the suggested target parameters.

$p^{\pm}$	$100 \quad KeV$
$e^{\mp}$	$54.46170 \quad eV$
γ	1.00010657887
β	0.0145987557
V	$4376596.86545\, m.s^{-1}$
τ	$0.57\, 10^{-3} \quad s$
$\sqrt{\frac{1+\beta}{1-\beta}}$	1.01470689052

Table 3
Set 3: $K(p^-)$ produced at CERN with the AD.

$p^{\pm}$	$5 \quad MeV$
$e^{\mp}$	$2.72308505 \quad KeV$
γ	1.00532894336
β	0.102826529
V	$30826617.9578\, m.s^{-1}$
τ	$81.1\, 10^{-6} \quad s$
$\sqrt{\frac{1+\beta}{1-\beta}}$	1.10870342938

Table 4
Set 4: boosted spectroscopy experiment.

$p^{\pm}$	$1.501235696 \quad GeV$
$e^{\mp}$	$817.598496 \quad KeV$
γ	2.6
β	0.923076923
V	$276731499.692\, m.s^{-1}$
τ	$9.03\, 10^{-6} \quad s$
$\sqrt{\frac{1+\beta}{1-\beta}}$	5

the TSR ring in Heidelberg [5] and with the MEIBE [4] apparatus at the University of Western Ontario used p^+ beams with a kinetic energy of 21 MeV and $330KeV$ respectively. These values are within the range defined by the parameter sets chosen here. These experiments have shown experimental evidence that laser induced radiative recombination works and is well described by the theoretical formulae.

The main differences are:

- the interaction length which is $1.5m$ at TSR and $8.6\,cm$ at MEIBE
- the beam temperature as it shall be discussed in the next section.

3. The recombination rate

The two reactions involved are the radiative recombination (RR = 1 & 2) and the laser induced radiative recombination (LIRR = 3 & 4).

$$p^+ + e^- \longrightarrow H(nl) + \gamma \quad (1)$$
$$p^- + e^+ \longrightarrow \tilde{H}(nl) + \gamma \quad (2)$$

$$p^+ + e^- + \gamma \longrightarrow H(nl) + 2\gamma \quad (3)$$
$$p^- + e^+ + \gamma \longrightarrow \tilde{H}(nl) + 2\gamma \quad (4)$$

The expected production rates of H and $\tilde{H}$ being the same, in the following computation, only the case of H is considered.

The notation is the following: $H(nl)$ is the atom in the state with principal quantum number n and orbital quantum number l. The energy of the ground level ($n = 1$) is the ionization energy, $E_0 = -13.6\,eV$. The photon energy E_γ matches the difference between the kinetic energy of e^- in the rest frame of p^+ and the energy of level n:

$$E_\gamma = h\nu = \frac{1}{2}mv_e^2 + \frac{|E_0|}{n^2} \quad (5)$$

In this formula we have only taken into account the principal quantum number because the spread in photon energy is dominated by the spread in e^- velocity. The separation between states sharing the same principal quantum number and having different orbital quantum numbers l is negligible in this case.

The RR rate in a given state level nl is given by:

$$r(n) = n_e N_p \frac{\tau}{\gamma}\alpha(nl) \quad (6)$$

Where:

- n_e is the e^- beam density,
- N_p is the number of p^+ in the beam,
- $\tau\,/\,\gamma$ is the time of flight seen in the p^+ rest frame,
- $\alpha(nl)$ is the recombination coefficient.

The recombination coefficient is computed from the e^- velocity distribution in the rest frame of the p^+ and from the recombination cross section:

$$\alpha(nl) = \int_0^\infty v_e\, f(v_e)\, \sigma_{rec}(nl)\, dv_e \quad (7)$$

The velocity distribution in the beams follows a Maxwell distribution and with the notations used in [2] we have:

$$f(v) = \frac{\exp[-(\frac{v_\perp}{\Delta_\perp})^2]\ \exp[-(\frac{v_\parallel}{\Delta_\parallel})^2]}{\Delta_\perp^2\ \Delta_\parallel\ \pi\ \sqrt{\pi}}\ v^2 \quad (8)$$
$$v_\perp = v^2\ \sin(\theta)^2 \quad v_\parallel = v\ \cos(\theta)$$

Where $\perp$ corresponds to the velocity projection in the transversal plane (x, y) and $\parallel$ corresponds to the velocity projection along the z axis. The temperatures in the transversal and longitudinal directions will be noted $T_\perp$ and $T_\parallel$. The temperatures correspond to kinetic energy distributions and will be estimated in energy units (meV) rather than Kelvins. The use of "kinetic energy" is reserved for single particles or for target beam energy.

Introducing the $erf(z)$ function, equation 7 can be rewritten in the form[1]:

[1] see [2] p256 eq 11 and 13

$$\alpha(nl) = \frac{2}{\Delta_\perp^2 \Delta_\parallel} \int_0^\infty \sigma_{rec}(nl)\ v^3 \exp\left(-(\frac{v_\perp}{\Delta_\perp})^2\right) \frac{erf(z)}{z} dv \quad (9)$$

Where z is defined by:

$$z = v\sqrt{\frac{1}{\Delta_\parallel^2} - \frac{1}{\Delta_\perp^2}} \quad (10)$$

In the following we will suppose that the beams have a "flattened" distribution: $\Delta_\parallel \ll \Delta_\perp$.

With this hypothesis, equation 10 becomes:

$$\alpha(nl) = \frac{2}{\Delta_\perp^2} \int_0^\infty \sigma_{rec}(nl)\ v^2 \exp\left(-(\frac{v_\perp}{\Delta_\perp})^2\right) dv \quad (11)$$

This integral is computed analytically in the appendix.

The LIRR process is similar to the stimulated emission of a photon with the difference that while stimulated emission occurs between two discrete quantum states, LIRR occurs between the continuum and a discrete state [2]. The same analogy can be drawn between the RR process and spontaneous emission. In the same way that spontaneous emission and stimulated emission probabilities are related by the Einstein relations, similar relations exist between RR and LIRR. If we define the gain $G(n)$ by the ratio of the LIRR and RR processes for a recombination into the atom with energy level n then:

$$G(n) = \frac{\sigma(LIRR)}{\sigma(RR)} = \frac{Pc^2}{F\Delta\nu 8\pi h\nu^3} \quad (12)$$

where:

- P is the laser power in Watts,
- F is the laser beam area cross-section
- ν is the laser frequency
- $\Delta\nu$ is computed from equation 5 and is dominated by the e^- kinetic energy spread (the atomic level width is negligible).

Therefore the LIRR rate is obtained from the RR rate computation.

It shall be noted that the LIRR process is limited by the photoionization when the photon flux increases: the atom, created by the LIRR process, is immediately destroyed by photoionization because both processes are induced by photons with the same wavelength.

The maximum photon flux Φ before saturation due to photoionization is given by:

$$\Phi = t_{min} \times \sigma_{phot}(n, \nu) \quad (13)$$

Where:

- t_{min} is the shorter of the laser pulse time length and the target state (nl) life time,
- $\sigma_{phot}(n, \nu)$ is the photoionization cross section for the atom at energy level n and with photons of frequency ν.

The TSR experiment has observed LIRR with the target state level $n = 2$ while the MEIBE experiment has observed LIRR with the target states $n = 11$ and $n = 12$. Depending on the target state, typical gains with conventional lasers are in the range $(50, 2000)$. It shall be noted that the experiment at TSR, due to a miss-alignment of the two beams, had an electrostatic field which enhanced the photoionization cross section[8–11], therefore limiting the gain. This effect does not appear when the beams are well aligned. In the configuration presented here, the $e^\mp$ beam will produce an electric field which is zero on the beam axis and reaches its maximum on the edge at a radius of approximatively $1\,cm$. In order to avoid the enhancement of the photoionization cross section, the laser light shall be concentrated within a diameter of $2 \sim 3\ mm$. As the RR rate will show, a gain of 50 is sufficient here.

4. Numerical results for the different sets

The target energy levels of the atom after recombination and their life time are given in table 5.

Table 5
12 first energy levels and life times of the (anti) hydrogen atom.

n	$E(eV)$	$\lambda(nm)$	$\tau_0(ns)$
1	-13.6	91.91	∞
2	-3.4	367.65	2.1
3	-1.5	833.30	10.2
4	-0.85	1470.60	33.5
5	-0.54	2314.80	88
6	-0.37	3308.80	196
7	-0.28	4503.60	81.2
8	-0.21	5882.40	108.3
9	-0.168	7444.80	173.5
10	-0.136	9191.10	238.3
11	-0.11	11121.30	317.6
12	-0.09	13235.20	412.7

The origin of the energy scale corresponds to the system of free particles $e + p$. The recombination emits a photon whose wavelength is in the 3rd column of table 5. After the recombination into the state (nl), the atom radiates photon(s) to reach the ground level. The life time of the atom [1] in the excited level (nl) is the 4th column in table 5 .

The target beam temperatures for this experiment are below 100 meV, therefore the values in column 2 show the excited states up to level 12. Above this level, excited states can be re-ionized by collisions and the number of atoms produced results from the competition between recombination and ionization. These states will not be taken into account for the estimation of the production rate. Hence the rates are slightly underestimated (less than a factor 2). The numerical results of the computation of the recombination coefficient $\alpha(nl)$ are presented in tables 6, 7 and 8 in units of $10^{-12}\ cm^3.s^{-1}$. The transversal beam temperature $T_\perp$ in meV is shown on top of each column.

The transversal beam temperature of $T_\perp = 200\ meV$ is included to be compared with the experimental value found at Novosibirsk [2,7]:

Table 6
$\alpha(nl)$ in units of $10^{-12}\ cm^3.s^{-1}$

n	$0.5\ meV$	$1.0\ meV$	$1.5\ meV$	$2.0\ meV$
1	10.716	7.577	6.187	5.358
2	4.286	3.031	2.475	2.143
3	4.072	2.879	2.351	2.036
4	3.372	2.383	1.945	1.684
5	2.697	1.906	1.556	1.347
6	2.247	1.588	1.296	1.121
7	1.926	1.360	1.110	0.960
8	1.684	1.190	0.970	0.839
9	1.497	1.057	0.862	0.745
10	1.347	0.950	0.775	0.670
11	1.224	0.863	0.703	0.608
12	1.121	0.791	0.644	0.556
Total	36.189	25.575	20.874	18.067

Table 7
$\alpha(nl)$ in units of $10^{-12}\ cm^3.s^{-1}$

n	$25\ meV$	$50\ meV$	$75\ meV$
1	1.5155	1.0716	0.8749
2	0.8335	0.5894	0.4811
3	0.5759	0.4072	0.3325
4	0.4703	0.3281	0.2646
5	0.3734	0.2588	0.2075
6	0.3084	0.2122	0.1691
7	0.2617	0.1787	0.1415
8	0.2264	0.1534	0.1208
9	0.1988	0.1337	0.1046
10	0.1767	0.1178	0.0917
11	0.1584	0.1048	0.0811
12	0.1433	0.0940	0.0724
Total	6.2423	3.6502	2.9418

Table 8
$\alpha(nl)$ in units of $10^{-12}\,cm^3.s^{-1}$

n	$100\,meV$	$200\,meV$
1	0.7577	0.5358
2	0.4167	0.2143
3	0.2879	0.2036
4	0.2264	0.1534
5	0.1767	0.1178
6	0.1432	0.0940
7	0.1193	0.0771
8	0.1013	0.0646
9	0.0873	-
10	0.0761	-
11	0.0671	-
12	-	-
Total	2.4597	1.4606

$1.46\,10^{-12}\,cm^3.s^{-1}$ versus $2.2\,10^{-12}\,cm^3.s^{-1}$. The difference is due to the limitation of the sum over the 8 levels which are not affected by re-ionization at that temperature while all levels participate in the experimental value.

In equation 6, the hypothesis on the number of $p^{\pm}$and the density of the $e^{\mp}$beam is that the product $n_e N_p = 5.\,10^{19}\,cm^{-3}$ (this hypothesis is discussed in the next section).

Then, the recombination coefficient values together with times of flight τ and the relativistic boost γ tabulated in tables 1 2 3 4 allows the computation of the number of recombined atoms produced at each burst in the vacuum pipe via equation 6.

The numbers obtained in table 9 show that, with a laser to set the gain at 50, 10^6 p^- can be recombined at any beam temperature below $200\,meV$ and a kinetic energy $K(p^{\pm})$= $100 KeV$. If we define the apparatus efficiency as the proportion of recombined p^-, then the efficiency is 100 %: all the p^- produced are used. In the long vacuum pipe configuration, the p^- are not recycled like in a storage ring but nevertheless they are all used. Furthermore, to keep p^- in a storage ring a very good vacuum has to be maintained.

Table 9
Millions of recombined atoms per burst without laser gain

$T_\perp$	$50\,KeV$	$100\,KeV$
$0.5\,meV$	1.46	1.03
$1.0\,meV$	1.03	0.73
$1.5\,meV$	0.84	0.59
$2.0\,meV$	0.73	0.51
$25\,meV$	0.252	0.178
$50\,meV$	0.147	0.104
$75\,meV$	0.119	0.084
$100\,meV$	0.099	0.070
$200\,meV$	0.059	0.042

Table 10
Millions of recombined atoms per burst without laser gain

$T_\perp$	$5\,MeV$	$1.5\,GeV$
$0.5\,meV$	0.14	0.006
$1.0\,meV$	0.10	0.004
$1.5\,meV$	0.08	0.0035
$2.0\,meV$	0.07	0.0031
$25\,meV$	0.025	0.0011
$50\,meV$	0.015	0.0006
$75\,meV$	0.012	0.0005
$100\,meV$	0.010	0.00042
$200\,meV$	0.006	0.00025

At the AD storage ring at CERN, the limitation of the number of p^- produced at each burst is due to the vacuum. The AD vacuum is approximatively $10^{-10}\,torr$ which corresponds to a residual gas density equal to that of the p^- beam ($\sim 2.\,10^7$ particles, $2\,mm$ diameter and $100\,m$ length). It shall be noted that the AD was built with recycled magnets that cannot be heated to remove adsorbed particles while a vacuum of approximatively $10^{-11}\,torr$ can be achieved for the system presented here. The total time spent in the AD by the p^- for deceleration and cooling is about $80\,s$. In the long vacuum pipe configuration, the time of flight is less than $10^{-3}\,s$ which allows much shorter beams without the limitation due to the residual gas. Another difference with storage rings, which continuously produce recombined atoms at low rate, is that the beams do not need to be in a stable state during the path in the long vacuum pipe: shorter dense beams which could not be kept in a storage ring can be packaged at the entry provided that their instability has a characteristic time larger than $10^{-3}\,s$. The last electron cooling in the AD takes 10^6 loops, that is $6\,s$. The cooler length is approximatively 10^{-2} of the total AD length, hence the transfer of heat between beams takes about $6.\,10^{-2}\,s$. In the long vacuum pipe, the beam heating due to the density will not have time to take place.

5. Focussing of the charged beams

Experimentally, there is no difficulty to produce e^- beams with a density of $5.\,10^{13}\,cm^{-3}$ and beams of p^+ with 10^6 particles. The situation for p^- and e^+ is more difficult: in order to be produced and collected, the p^- requires a p^+ primary beam above $\approx 12\,GeV$. The e^+ are easier to produce and bursts of 10^{13} particles have been achieved at SLAC where bursts with more particles are foreseen.

With these numbers, the density of e^+ is seven orders of magnitude larger than the density of p^- particles: the two superposed beams can be considered as "a pure e^+ beam". At a p^+ kinetic energy of $100\,keV$, the corresponding e^- kinetic energy is only $54.4\,eV$. There are two consequences:

- the e^+ beam is destroyed by its internal electric field,
- no focussing can be applied to compensate for this field.

To cure this problem, a third beam of e^- is superposed to compensate the space charge so that a weak axial magnetic field can guide the beams.

The superposition of an e^- beam with an e^+ beam at low temperature produces positronium atoms. There are three reactions to be considered:

$$p^- + P_s \longrightarrow \tilde{H}(nl) + e^- \tag{14}$$

$$e^- + e^+ \longrightarrow P_s + \gamma \tag{15}$$

$$P_s \longrightarrow \gamma \tag{16}$$

Computations [34,35] confirmed by an experiment [36] have shown that in the temperatures range considered here, the cross section [2] of the reaction 14 is about $10\,\pi a_0^2 \sim 10^{-15}\,cm^2$. This is 10000 times larger than the RR cross section. Therefore, the positronium enhances the production of $\tilde{H}$.

The cross section of the reaction 15 is the same as the RR cross section of the e-p recombination provided that the ionization energy is replaced by the one of positronium. Hence this cross section is about 1/2 of the RR cross section:

$$\alpha_{e-e} = \frac{1}{2}\,\alpha_{e-p} \tag{17}$$

In the singlet spin state, the life time of positronium $P_s(1s)$ is $0.142\,ns$. In the triplet spin state, the life time is $142\,ns$. Therefore, the reaction 16 removes e^+ from the beam.

Since the positronium is about 10000 times more effective for producing $\tilde{H}$ but lives approximatively $100\,ns$, the positronium is equivalent to the presence of an e^+ particle during $1\,ms$, that is during the time of flight in the pipe.

Since the wavelength of the laser which sets the gain is tuned for the e-p reaction, if the beam of e^+ particles is neutralized by a beam of e^-, then most of the $H/\tilde{H}$ production is done through the

[2] where $a_0 = 0.529\,10^{-10}\,m$ is the Bohr radius

e-p channel. For instance, at a temperature of $10 meV$, $\alpha_{e-p} \sim 10^{-11} cm^2$, hence the probability for a $p^{\pm}$to be recombined during a $1\ ms$ flight is approximatively:

$$\alpha_{e-p} \times n_e \times 10^{-3} = 10\,\% \tag{18}$$

And the probability for producing a P_s is approximatively 5 %. With a gain set at $G = 10$ the production of $H/\tilde{H}$ is 20 times more likely to happend through the e-p channel than through the P_s channel. The total number of $e^{\mp}$absorbed by the production of P_s is only 5 % of the total. Therefore, the beam neutralization, while important for keeping the charged beams in the pipe, plays only a small role in the $H/\tilde{H}$ production.

6. Focussing of the anti-atom or atom beam

The recombined atoms are produced all along the pipe and, depending on the transversal beam temperature, they may or may not need guiding devices to reach the exit without interacting with the pipe. Table 11 shows the average transversal distance at the pipe exit (in cm) for the atoms created at the entry: it gives the radius of the cone inside which the atoms would be after a $2500\ m$ flight, if no focussing device is installed.

Since the atoms are on the ground level, and since there is no laser available with a wave length of $121 nm$ it is not possible to use Doppler shifted stimulated emission of the one-photon 1s-2p transition for transferring transversal quanta of momentum to focus the beam.

Therefore it is proposed to use the hyperfine (hfs) structure of the 1s energy level. This transition is used in MASER experiments where few atoms in the ground level excite a spherical cavity tuned on the hfs transition (1.420 Ghz) which, in turn, produces stimulated emission of the other atoms, generating the measured electric signal. The focussing device is a MASER operated in reverse mode: the electric signal is not extracted but injected in the cavity. The cavity is excited in the TE101 mode at a frequency Doppler shifted so that the atoms with transverse velocity transfer transverse momentum to the electromagnetic field in the cavity by stimulated emission. Several shapes can be selected for the cavity: spherical, cylindrical, rectangular. For MASER experiments the spherical shape is often selected and will be taken as practical example. The mode to be excited, TE101, is shown in figure 2. For this mode a cavity made of copper has the following parameters:

- the sphere radius a,
- the electrical resistance R_s,
- the quality coefficient Q,
- the frequency width $\Delta\,\nu$.

This mode is the superposition of spherical waves travelling from the z axis to the edge and from the edge to the z axis. The cavity is tuned with a Doppler shift so that the atoms with transverse momentum are within the resonance while the other ones are de-tuned. This is possible due to the width of the mode which is slightly larger than the Doppler shift for an atom with kinetic energy of $200\,meV$. The transversal velocity and the corresponding Doppler shift for different temperatures is presented in table 13.

Table 11
Atom beam cone radius (without focussing) at the exit in cm

$T_\perp$	$50\ KeV$	$100\ KeV$	$5\ MeV$	$1.5\,GeV$
$0.1\,meV$	11.2	7.9	1.1	0.1
$0.2\,meV$	15.8	11.2	1.6	0.2
$0.5\,meV$	25.0	17.6	2.5	0.3
$1.0\,meV$	35.4	24.9	3.5	0.4
$2.0\,meV$	50.0	35.3	5.0	0.6
$5.0\,meV$	79.1	55.8	7.9	0.9
$10\,meV$	111.8	78.9	11.2	1.2
$20\,meV$	158.2	111.6	15.9	1.8
$50\,meV$	250.1	176.4	25.1	2.8
$100\,meV$	353.7	249.5	35.5	3.9
$150\,meV$	433.1	305.6	43.5	4.8
$200\,meV$	500.1	352.8	50.2	5.6

One can see in figure 3 that, when the cavity tune is shifted by $29328 Hz$, atoms with no transversal velocity are de-tuned.

The crossing of the cavity for a beam with kinetic energy of $100\,KeV$ takes $96\,ns$ during which the field in the cavity oscillates 136.3 times. By shifting the beam target energy to $99.56\,KeV$ the number of oscillations is exactly 136 therefore the charged particles moving together with the atoms will not receive or lose energy during the crossing. Furthermore, the electric field on the z axis is $E = 0\ V.m^{-1}$ and the p^- beam is only $2\,mm$ in diameter while the e^+ beam is $1\,cm$ in diameter. At a distance of $1\,cm$ in the transversal plane, the field is only $\approx 5\ 10^{-3} \times E_{max}$ and the e^+ are guided by the axial magnetic field both inside the cavity (oscillating field) and outside. Hence, crossing the cavity shall create only negligible perturbations of the charged beams.

The focussing power of the cavity is limited by the 136 field oscillations. Each oscillation corresponds to one stimulated emission and each hfs photon has an energy of $5.87\ 10^{-6}\ eV$, therefore the transversal kinetic energy of the atom is decreased by $136 \times 5.87\ 10^{-6} eV = 0.798\,meV$. This gives the focussing power of a single cavity and allows the computation of the number of cavities needed to remove the transversal kinetic energy. These numbers are summarized in table 14 which contains for each kinetic energy, the number of stimulated emissions and the corresponding number of cavities.

The electromagnetic power required to force the atoms'spin to oscillate 136 times is less than a few Watts. This is due to the life time of the upper hfs energy level which is very long: $\tau \sim 1s$. If A and B are the Einstein coefficients for spontaneous emision and absorption then:

$$A = \frac{1}{\tau} = 1 \quad B = \frac{A\,\lambda^3}{8\,\pi\,h} = 5.6\ 10^{29} \tag{19}$$

Therefore, the spontaneous emission is negligible and the number of transitions per unit time is given by:

$$dN = -N\ B\ \rho_\nu\ dt \tag{20}$$

Table 12
Spherical cavity parameters for the mode TE101

ν_{hfs}	$1420405751.768\,Hz$
$a = \frac{\lambda_{hfs}}{1.39}$	$15.18\,cm$
$R_s = 2.6\ 10^{-17}\ \sqrt{\nu_{hfs}}$	$9.8\ 10^{-3}\ \Omega$
$Q = \frac{1}{R_s}\sqrt{\frac{\mu_0}{\epsilon_0}}$	38473.508
$\Delta\,\nu = \frac{\nu_{hfs}}{Q}$	$36919.06\,Hz$

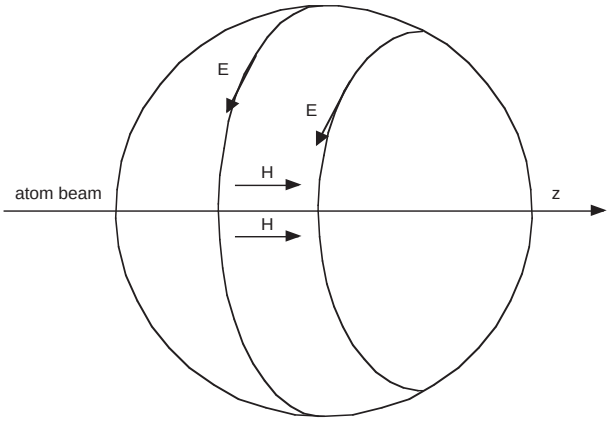

Figure 2. Field in a spherical cavity excited in the TE101 mode: the beam crosses the cavity along the z axis. Atoms with transverse momentum recoil from the stimulated emission of hfs photons.

The energy density in the cavity is:

$$\rho_\nu = \frac{1}{2}\epsilon_0\ E(\nu)^2 + \frac{1}{2}\mu_0\ H(\nu)^2 \tag{21}$$

For a field of $1\ V/m$, this leads to a transition characteristic time:

$$\frac{1}{B\ \rho_\nu} = \frac{1}{10^{-12} \times 10^{29}} = 10^{-17}\ s \tag{22}$$

In other words, even with a weak field of about $1 V/m$ the atoms spin follows the field oscillations.

7. Experimental configurations

The long vacuum pipe configuration brings specific capabilities which are difficult to achieve oth-

Table 13
Velocity and Doppler shift

$T_\perp$	$V\ m.s^{-1}$	$\Delta\ \nu_{hfs}\ Hz$
$0.1\ meV$	138.41	655.8
$0.2\ meV$	195.74	927.4
$0.5\ meV$	309.50	1466.4
$1.0\ meV$	437.70	2073.8
$2.0\ meV$	619.00	2932.8
$5.0\ meV$	978.71	4637.1
$10\ meV$	1384.11	6557.9
$20\ meV$	1957.43	9274.2
$50\ meV$	3094.97	14663.9
$100\ meV$	4376.95	20738.0
$150\ meV$	5360.64	25398.7
$200\ meV$	6189.94	29328.0

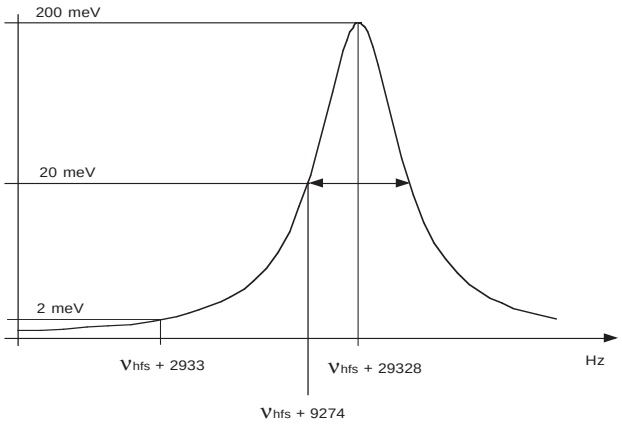

Figure 3. Doppler shift of the atoms according to their transversal kinetic energy

Table 14
Focussing power needed as a function of temperature

$T_\perp$	$nb\ h\nu_{hfs}$	$nb\ cavities$
$100\ meV$	17023	125
$50\ meV$	8511	63
$20\ meV$	3405	25
$10\ meV$	1702	16
$5\ meV$	851	6
$2\ meV$	340	3
$1\ meV$	170	2
$0.5\ meV$	85	1
$0.2\ meV$	34	1
$0.1\ meV$	17	1

erwise. They will be illustrated for three experiments:

- the Lamb shift measurement,
- the boosted spectroscopy,
- the gravitational mass measurement.

7.1. The Lamb shift measurement

Precise measurements of the Lamb shift in atomic hydrogen were obtained using the technique of the Separated Oscillatory Field [12–17] for the level $n = 2$.

Extensive reviews on this technique have been published. These measurements are among the most stringent tests of QED. In the SOF experiment, the difficulty is to produce a cold beam of atomic hydrogen with a kinetic energy in the $100\ keV$ range from which atoms in the state $2S_{1/2}(F = 0)$ are extracted and used for the interferometry. These beams are produced with a small proton accelerator followed by recombination into atoms through charge exchange collisions with nitrogen gas. The two advantages of using $e^- p^+$ recombination instead of charge exchange are:

- the number of atoms with energy level $n = 2$ can be enhanced with laser induced gain as in the TSR experiment,

Table 15
Number of recombined atoms in the $2S$ state per burst without laser gain

$T_\perp$	$50\ KeV$	$100\ KeV$
$0.5\ meV$	64939	45811
$1.0\ meV$	45917	32392
$1.5\ meV$	37493	26449
$2.0\ meV$	32469	22905
$25\ meV$	9184	6479
$50\ meV$	6494	4581
$75\ meV$	5302	3740
$100\ meV$	4592	3239
$200\ meV$	3247	2290

- the beam temperature can be lower ($1\,meV$ corresponds to $11.6\ K$).

The first feature could be used in a storage ring but it is counter-balanced by the very small rate of atoms produced. The long vacuum pipe configuration does not have this limitation. In the case of p^+, the number of atoms is only limited by the acceleration to $100\,keV$. Contrary to the charge exchange process, there are no losses in the nitrogen gas. In the case of p^- tables 15 and 16 show the number of atoms produced in the $2S$ state per burst: these numbers can be enhanced by a factor ≈ 50 with a laser. Finally the long vacuum pipe configuration allows the measurement to be made on matter and anti-matter produced in the same conditions: the relative comparison of the Lamb shift is free from systematic effects related to the anti-matter production.

7.2. The boosted spectroscopy

The possibility of producing H and $\tilde{H}$ beams at a kinetic energy of $1.5\ GeV$ suggests a new type of spectroscopy. This kinetic energy corresponds to table 4. Let's consider the configuration shown in figure 4.

The light frequency in the laboratory reference frame and in the beam reference frame are referred to as follows:

- ν_0 is the frequency of the light, emitted by the laser, in the laboratory reference frame,
- ν_1 is the frequency of the light in the atom

Table 16
Number of recombined atoms in the $2S$ state per burst without laser gain

$T_\perp$	$5\ MeV$	$1.5\ GeV$
$0.5\ meV$	6518	279
$1.0\ meV$	4609	197
$1.5\ meV$	3763	161
$2.0\ meV$	3259	140
$25\ meV$	922	39
$50\ meV$	652	28
$75\ meV$	532	23
$100\ meV$	461	20
$200\ meV$	326	14

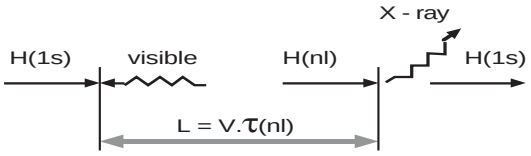

Figure 4. Source and echo in boosted spectroscopy

reference frame,

- ν_2 is the frequency of the light emitted by the atom, in the laboratory reference frame.

These frequencies are related by:

$$\nu_2 = \sqrt{\frac{1+\beta}{1-\beta}} \times \nu_1 \tag{23}$$

$$\nu_1 = \sqrt{\frac{1+\beta}{1-\beta}} \times \nu_0 \tag{24}$$

$$\nu_2 = \frac{1+\beta}{1-\beta} \times \nu_0 \tag{25}$$

The large Doppler factor (= 5) allows the use of common lasers with wave lengths in the visible range $\lambda \approx 500\,nm$ to excite any state from the ground state. Conversely, the light re-emitted from the atom in the transition to the ground state is seen in the laboratory reference frame as X-rays with $\lambda \approx 25\,nm$. In the following, the excitation light at $\lambda \approx 500\,nm$ is called the *source*, while the X-rays with $\lambda \approx 25\,nm$ are called the *echo*. Two measurements are available:

- the energy level of an excited state,
- the life time of the excited state.

To measure the energy level of an excited state, the source wave length is carefully tuned around the transition while the intensity of the echo is recorded. A fit on the intensity curve is made to locate the maximum and the corresponding wavelength of the source gives the energy of the level.

To measure the life time, the point where the laser is focused and the atoms are excited is scanned until the intensity of the echo is maximum: the time of flight of the atoms between this point and the detection region is equal to the life time of the excited states multiplied by the relativist boost $\gamma = 2.6$.

In the first measurement, the precision is limited by the velocity spread of the atoms:

$$\frac{\Delta\nu_2}{\nu_2} = \frac{\Delta\nu_0}{\nu_0} + \frac{2\,\Delta\beta}{1-\beta^2} \tag{26}$$

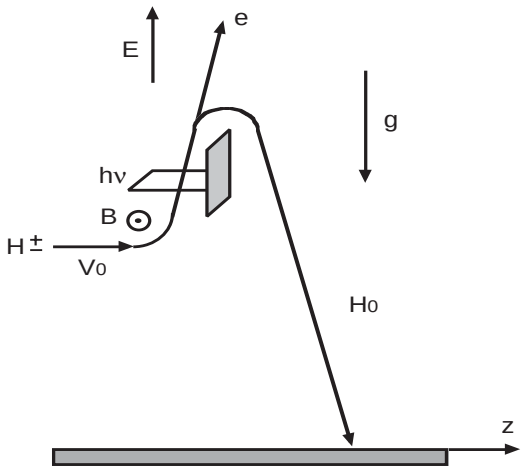

Figure 5. Gravitational mass experiment

If we take the same velocity spread as in the TSR experiment then $\Delta\beta = 2\ 10^{-4}$. Inserting it into equation 26 and considering that the excited states of the hydrogen are at $\approx 10\,eV$ the error on the energy level is given by:

$$\Delta h\nu_2 = \Delta h\nu_0 + 27\ meV \tag{27}$$

In the second measurement, if the maximum is located with $1\,cm$ precision, then since the atom velocity is $2.7\ 10^8\,m.s^{-1}$ the error is $\approx 0.037\,ns$.

In table 10 the number of anti-hydrogen atoms produced at a temperature of $25\ meV$ is 1100, but this number can be easily enhanced by a factor ≈ 20 with a laser induced gain. These anti-hydrogen atoms are collimated in a cone of radius equal to $1.8\,cm$ according to table 11. With these parameters there is no difficulty in detecting the X-rays of the echo signal. Furthermore, due to the boost, 80 % of the echo light is emitted in the forward direction of the beam in the laboratory reference frame. Simple detectors made of scintillators leading to photomultipliers can collect the signal: no unconventional technology is required.

7.3. The gravitational mass measurement

The anti-matter mass measurements performed until now are performed on elementary charged particles trapped in a magnetic field: they are inertial mass measurements [21]. Experiments are underway, [20,22] where p^- and e^+ plasma are cooled, and then merged, to produce $\tilde{H}$ nearly at rest in the laboratory frame. It might be possible then, to perform gravitational mass experiments. The long vacuum pipe configuration offers another path to perform this experiment using the $\tilde{H}^+$ ion. Since the recombination of p^- and e^+ takes place inside an e^+ beam, some of the $\tilde{H}$ atoms produced capture an e^+ to form the $\tilde{H}^+$ ion. The $\tilde{H}^+$ ion can then be slowed down to a velocity of a few $cm.s^{-1}$ and manipulated before the e^+ is removed by a laser pulse. The acceleration and manipulation of the ion has been performed [23] in the past up to $800\,MeV$ and there is no difficulty in decelerating, manipulating and removing the e^+.

The experience is shown in figure 5. The notations are as follows:

- V_0 is the ion velocity,
- B is the magnetic field to tune the parabolic flight,
- g is the gravitational field,
- E is a weak electrostatic field that is used to remove the e^+,
- $h\nu$ is the laser light used to separate $\tilde{H}$ from e^+
- $\tilde{H}_0$ is the atom in the ground state,
- z is the distance before $\tilde{H}$ reaches the detector.

The magnetic field and the initial velocity allows to tune the parabolic flight. The e^+ is separated from the $\tilde{H}$ by a laser with a wave length slightly below the binding energy ($0.75\,eV$) and a mirror so that the separation is made through a two photon process. In such a process, the ion can absorb the two photons in three different ways:

- the two photons come from the laser,
- the two photons come from the mirror,
- one photon comes from each side.

Therefore there can be momentum transfer from each of the sides or no transfer at all giving three separated signals along the z axis. These signals allow to monitor the effect of the laser and to avoid systematic effects due to momentum transfer during the separation.

The magnetic field, the velocity and the distance are sufficient to make the gravitational mass measurement but another parameter can be added to obtain redundancy. The laser can be pulsed to define the starting time of the flight and the time of flight can be detected when the atom reaches the detector.

Such a configuration allows to make a free fall experiment, atom per atom without interference with residual electric fields since the atoms are neutral.

The radiative attachment cross-section is known theoretically and experimentally with precision [18] due to its important role in astrophysics observations and its values are shown in table 17. This cross-section tends to zero when the kinetic energy of the e^+ decreases toward zero. The kinetic energy is taken in the reference frame of the atom. To choose a suitable kinetic energy for e^+, one has to take into account the affinity $e-H$ which is equal to $0.75eV$. Above this energy, the ions start to be dismantled by e^+ col-

Table 17
$\sigma(e^+ + \tilde{H} \rightarrow \tilde{H}^+) = \sigma(e^- + H \rightarrow H^-)$

e^+ kinetic energy (eV)	cross-section $\times 10^{-22}\,cm^2$
0.135	0.456
0.406	0.570
0.677	0.583
1.354	0.547
2.708	0.455
5.416	0.315
8.124	0.300
10.832	0.270

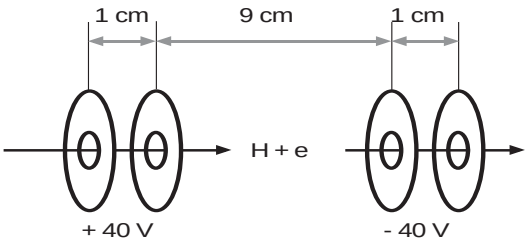

Figure 6. One pair of electrostatic cells for ion production

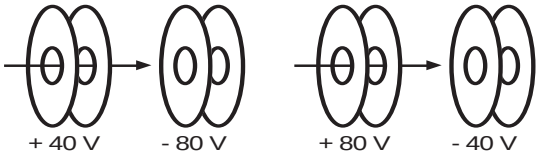

Figure 7. Stack of electrostatic cells for ion production

lisions. The chosen compromise is to operate at a kinetic energy of $0.4\,eV$. This energy is achieved by pairs of electrostatic cells of $1\,cm$ length with an electric potential of $40\,V$ as shown in figure 6. The cells are separated by a space without field, the length of which is $9\,cm$. It is in that space that the ion production takes place. Since the kinetic energy gained in one cell is compensated in the next one, the e^+ kinetic energy is unchanged after crossing one pair of cells.

If several pairs of cells are stacked, then to avoid cummulative delay between the e^+ beam and the $\tilde{H}$ beam, the direction of the electric field is alternated, hence the internal cells have an electric potential of $80\,Volts$ as shown in figure 7.

The number of ions produced between a pair of cells is computed with the following approximation: the kinetic energy of e^+ is constant and equal to $0.4\,eV$ (the spread of kinetic energy in the e^+ beam is few meV and it is neglected).

The parameters are:

- velocity of the e^+ in the $\tilde{H}$ reference frame: $V = 375107\,m.s^{-1}$,
- active length of the cell: $L = 9\,cm$,
- density of e^+: $n_e = 5\,10^{13}\,cm^{-3}$,
- number of $\tilde{H}$: $N_{\tilde{H}} = 10^6$,
- the cross-section: $Q = 0.570\,10^{-22}\,cm^2$,
- the relativistic boost $\gamma = 1$.

The number of ions produced in each cell is given by:

$$N(\tilde{H}^+) = n_e\,N_{\tilde{H}}\,\frac{L}{V}\,Q = 0.02565 \qquad (28)$$

Over a length of $100\,m$ the number of cells is 1000. Then the number of ions $\tilde{H}^+$ produced per burst is: $N(\tilde{H}^+) = 25.65$.

8. The production of p^-

The hypotheses for the production of antiproton beams are based on the the Antiproton Decelerator (AD) operated at CERN [24,25]. The main characteristics of the AD are presented now.

The parameters of the primary beam of p^+ are:

- momentum: $26\,GeV/c$,
- diameter: $1\,mm$,
- number of particles per pulse: $1.5\,10^{13}$

This beam interacts with an iridium target to produce p^- which are collected in a magnetic horn [26]. The interaction produces $5.10^7 p^-$ with a momentum of $3.5\,GeV$. The limit to avoid the target destruction is $6.10^{14}\,p^+$ per GeV/c which corresponds to $2.5\,10^{13}$ for the CERN p^+ beam. After being collected, the p^- are alternatively cooled and decelerated. There are two stochastic cooling steps and two electron cooling steps. Finally the p^- beam is delivered to the experiments with a momentum of $100\,MeV/c$ (kinetic energy of $5\,MeV$) and a momentum spread of

$\Delta p/p \approx 5.10^{-4}$. The AD delivers pulses of approximatively $3.10^7\ p^-$.

After the AD, the ASACUSA experiment [27] uses an inverted Linac which further reduces the kinetic energy to approximatively $63 \pm 60\ keV$. This last deceleration has a yield of 40%.

The main limitation of the AD comes from the fact that it cannot be heated to remove adsorbed particles and the vacuum is $10^{-10}\ torr$. There is no use to further cool down the p^- beam because the collisions with the residual gas heat the beam. The beam temperature is approximatively $200\ meV$.

On ion storage ring experiments, electrons with a temperature of $10 \sim 20\ meV$ are obtained with inhomogeneous magnetic fields. These electrons can be used to further cool down a p^- beam, provided that there are no other effects which heat the beam.

At low temperature, below few meV, beams are expected to reach a crystalline state [31] where the relative positions of the particles in the beam is constant. Studies [29] have shown that in a machine where the particles are focussed with an alternating gradient quadrupole system (4-AG), the intrabeam scattering and the space-charge tune shift prevent the crystalline state to be created. Conversely, it is predicted [30] that if alternating gradient octupoles (8-AG) are used these limitations can be removed. In the case of $e^{\mp}$, an alternative design was proposed where the particles are guided along a strong magnetic field: a machine of this type, called LEPTA [32,33], is being built at the Joint Institute for Nuclear Research in Dubna, Russia. The first experimental results are expected in 2002.

From the AD parameters and from the study of an anti-proton accumulation and deceleration ring at KEK in Japan [28], an extrapolation shows that for the production of beams with $10^5 \sim 10^6\ p^-$, a primary beam of $3.10^{13}\ p^+$ at $12 \sim 14\ GeV$ is required. This beam would be produced in two steps:

- a first accelerator ring up to $4\ GeV$ to produce relativistic p^+,
- a second accelerator to boost the energy to $12 \sim 14\ GeV$.

No technical novelty is required for the second accelerator.

At $12 \sim 14\ GeV$, the p^- are produced with a momentum of $2 \sim 3\ GeV/c$ and the collection and deceleration scheme would be similar to that of the AD. But the cooling/deceleration would be extended further to create crystalline beams. The first accelerator shall also be used as the decelerator. In order to reach lower temperature, it shall be an octupole machine where p^- beams can reach the crystalline state. The e^+ would be cooled and stored in a small ring (length of $\approx 20\ m$) similar to LEPTA.

9. Conclusion: target parameters

The experimental configuration presented in this article allows to produce atoms of antihydrogen in the form of beams. The computations lead to the following target parameters for the proposed experiments:

- p^- kinetic energy: $K(p^-) = 100\ keV$,
- number of p^- particles per beam: $N_p = 10^6$,
- density of the e^+ particles: 5.10^{13},
- temperature of the p^- and e^+ beams: $T \leq 5\ meV$.

These parameters can be relaxed by increasing the gain from 10 to 500: the density of $e^{\mp}$can be relaxed by 1 or 2 order of magnitude, the kinetic energy of the $p^{\pm}$can be increased up to 5$\sim$100 MeV and the temperature up to 100 meV.

For the boosted spectroscopy experiment the target kinetic energy is $1.5\ GeV$.

10. Acknowledgments

I wish to thanks D. Möhl and S. Maury from the CERN AD group who have guided me in the comprehension of the Antiproton Decelerator operation and who have suggested to look into crystalline beams. I wish to thanks also I. N. Meshkov for explaining and presenting me the status of electron cooling. I am grateful to Chi-Yu Hu who carefully presented the use of positronium

to produce antihydrogen at the poster session of the ICPEAC 2001 conference. I am grateful to P. Perez who have taken the burden to check the computations and for the fruitfull discussions we had. I thanks P. Debu and his deputy G. CozziKa who head the DAPNIA-SPP lab and who have strongly encouraged this work.

11. Appendix

The recombination coefficient $\alpha(nl)$ is given by:

$$\alpha(nl) = \frac{2}{\Delta_\perp^2} \int_0^\infty \sigma_{rec}(nl)\ v^2 \exp\left(-\left(\frac{v_\perp}{\Delta_\perp}\right)^2\right) dv \quad (29)$$

For $n = 1$ the cross-section $\sigma_{rec}(1)$ can be approximated [2] by:

$$\sigma_{rec}(1) = \frac{E_0}{E_e}\, 1.676\, 10^{-22}\, cm^2 \quad (30)$$

Where E_0 is the ionization energy, $13.6\, eV$ and E_e is the e^- kinetic energy.

For $n \leq 3$ the cross-sections are given by:

$$\sigma_{rec}(2) = 0.550 \times \sigma_{rec}(1) \quad (31)$$
$$\sigma_{rec}(2s) = 0.15 \times \sigma_{rec}(1) \quad (32)$$
$$\sigma_{rec}(2p) = 0.40 \times \sigma_{rec}(1) \quad (33)$$
$$\sigma_{rec}(3) = 0.380 \times \sigma_{rec}(1) \quad (34)$$
$$\sigma_{rec}(3s) = 0.05 \times \sigma_{rec}(1) \quad (35)$$
$$\sigma_{rec}(3p) = 0.153 \times \sigma_{rec}(1) \quad (36)$$
$$\sigma_{rec}(3d) = 0.177 \times \sigma_{rec}(1) \quad (37)$$

Therefore the recombination coefficients for $n \leq 3$ are obtained from the value of the integral:

$$I_1 = \int_0^\infty \frac{2}{\Delta_\perp^2} \cdot \frac{v^2 E_0}{\frac{1}{2} m_e v^2} \cdot \exp\left(-\left(\frac{v}{\Delta_\perp}\right)^2\right) dv \quad (38)$$

$$I_1 = \int_0^\infty \frac{4\, E_0}{\Delta_\perp^2\, m_e} \cdot \exp\left(-\left(\frac{v}{\Delta_\perp}\right)^2\right) dv \quad (39)$$

$$x = \frac{v}{\Delta_\perp} \quad dv = \Delta_\perp\, dx \quad (40)$$

$$I_1 = \frac{4\, E_0}{\Delta_\perp\, m_e} \int_0^\infty e^{-x^2} dx \quad (41)$$

$$t = x^2 \quad dx = \frac{dt}{2\sqrt{t}} \quad (42)$$

$$I_1 = \frac{4\, E_0}{\Delta_\perp\, m_e} \int_0^\infty e^{-t} \frac{dt}{2\sqrt{t}} \quad (43)$$

$$\int_0^\infty e^{-t} \frac{dt}{2\sqrt{t}} = \frac{1}{2}\, \Gamma\left(\frac{1}{2}\right) = \frac{\sqrt{\pi}}{2} \quad (44)$$

Finally:

$$\alpha(1) = \frac{2\, E_0\, \sqrt{\pi}}{\Delta_\perp\, m_e} \times 1.676\, 10^{-26}\, m^3.s^{-1} \quad (45)$$

For $n > 3$ the cross-section $\sigma_{rec}(n)$ can be approximated [2] by:

$$\sigma_{rec}(n, E_e) = \frac{E_0^2 \times 2.11\, 10^{-22}\, cm^2}{n\, E_e (E_0 + n^2 E_e)} \quad (46)$$

This expression can be split into two parts:

$$\frac{1}{E_e(E_0 + n^2 E_e)} = \frac{A}{E_e} + \frac{B}{E_0 + n^2 E_e} \quad (47)$$

with

$$A = \frac{1}{E_0} \quad B = -\frac{n^2}{E_0} \quad (48)$$

The recombination coefficients for $n > 3$ are obtained from the value of the integral:

$$\alpha(n) = \int_0^\infty \frac{2}{\Delta_\perp^2} \sigma_{rec}(n, E_e) v^2 \exp\left(-\left(\frac{v}{\Delta_\perp}\right)^2\right) dv \quad (49)$$

$$E_e = \frac{1}{2}mv^2 \quad dv = \frac{1}{\sqrt{2m}}\frac{dE_e}{\sqrt{E_e}} \tag{50}$$

$$\alpha(n) = \frac{2}{\Delta_\perp^2} \times \frac{2}{m} \times \frac{1}{\sqrt{2m}} \times \tag{51}$$
$$\int_0^\infty \sigma_{rec}(n, E_e)\, \sqrt{E_e}\, \exp\left(-\frac{2E_e}{m\Delta_\perp^2}\right)\, dE_e$$

$$x = \frac{2E_e}{m\Delta_\perp^2} \quad dE_e = \frac{m\Delta_\perp^2}{2}dx \tag{52}$$

$$\alpha(n) = \Delta_\perp \int_0^\infty \sigma_{rec}(n, x)\, \sqrt{x}\, e^{-x}\, dx \tag{53}$$

$$\alpha(n) = 2.11\, 10^{-22}\, cm^2 \times \frac{\Delta_\perp\, E_0^2}{n} \times I_n \tag{54}$$

And $I_n = I_A + I_B$ with:

$$I_A = \frac{2\, A}{m\, \Delta_\perp^2} \int_0^\infty \frac{1}{\sqrt{x}}\, e^{-x}\, dx \tag{55}$$

$$I_A = \frac{2\, A}{m\, \Delta_\perp^2}\, \Gamma\left(\frac{1}{2}\right) = \frac{2\sqrt{\pi}}{m\, E_0\, \Delta_\perp^2} \tag{56}$$

$$I_B = B \int_0^\infty \frac{1}{E_0 + \frac{n^2\, m\, \Delta_\perp^2\, x}{2}} \sqrt{x}\, e^{-x}\, dx \tag{57}$$

$$u = E_0 + \frac{m\, n^2\, \Delta_\perp^2}{2}\, x \tag{58}$$

$$x = (u - E_0) \times \frac{2}{m\, n^2\, \Delta_\perp^2} \tag{59}$$

$$dx = \frac{2}{m\, n^2\, \Delta_\perp^2}\, du \tag{60}$$

$$I_B = B \cdot \frac{2}{m\, n^2\, \Delta_\perp^2} \cdot \sqrt{\frac{2}{m}} \cdot \frac{1}{n\, \Delta_\perp} \times \tag{61}$$
$$\int_0^\infty \frac{\sqrt{u - E_0}}{u}\, \exp\left(-\frac{2\,(u - E_0)}{m\, n^2\, \Delta_\perp^2}\right) du$$

$$t = u - E_0 \quad a = \frac{2}{m\, n^2\, \Delta_\perp^2} \tag{62}$$

$$I_B = B \cdot \frac{2}{m\, n^2\, \Delta_\perp^2} \cdot \sqrt{\frac{2}{m}} \cdot \frac{1}{n\, \Delta_\perp} \times \tag{63}$$
$$\int_0^\infty \frac{\sqrt{t}}{E_0 + t} \cdot e^{-at}\, dt$$

$$u = \sqrt{t} \quad dt = 2\, u\, du \tag{64}$$

$$\int_0^\infty \frac{\sqrt{t}}{E_0 + t} e^{-at} dt = \int_0^\infty \frac{2u^2}{E_0 + u^2} e^{-au^2} du \tag{65}$$

$$= 2\int_0^\infty e^{-au^2} du - 2\int_0^\infty \frac{E_0}{E_0 + u^2} e^{-au^2} du \tag{66}$$

Using the formula 7.4.11, 6.1.1 and 6.1.8 from the "Handbook of Mathematical Functions" [3], one gets:

$$\int_0^\infty \frac{E_0}{E_0 + u^2} \cdot e^{-au^2} du \tag{67}$$
$$= \frac{\pi}{2} \cdot \sqrt{E_0} \cdot e^{aE_0} \cdot erfc(\sqrt{aE_0})$$

$$\int_0^\infty e^{-au^2} du = \int_0^\infty \frac{1}{\sqrt{t}} e^{-at} dt \tag{68}$$
$$= \frac{1}{2\sqrt{a}} \cdot \Gamma\left(\frac{1}{2}\right) = \frac{1}{2}\sqrt{\frac{\pi}{a}}$$

Grouping the two integrals and replacing B by its value leads to:

$$I_B = -\frac{n^2}{E_0} \cdot a \cdot \sqrt{\frac{2}{m}} \cdot \frac{1}{n\,\Delta_\perp} \times \left(\sqrt{\frac{\pi}{a}} - \pi\,\sqrt{E_0}\,e^{aE_0}\,erfc(\sqrt{aE_0}) \right) \tag{69}$$

Summing I_A and I_B and replacing a by its value in the factorization gives a cancellation of the two largest terms:

$$\frac{\Delta_\perp\,E_0^2}{n} \times I_n = \frac{2\sqrt{\pi}\,E_0}{n\,m\,\Delta_\perp} - \frac{2\sqrt{\pi}\,E_0}{n\,m\,\Delta_\perp} + \frac{2\sqrt{2}\,\pi\,E_0\,\sqrt{E_0}}{n^2\,m\,\sqrt{m}\,\Delta_\perp^2} \cdot e^{aE_0} \cdot erfc(\sqrt{aE_0}) \tag{70}$$

Finally combining equations 54 and 70 gives the recombination coefficients for $n > 3$:

$$\alpha(n) = 2.11\,10^{-26}\,m^2 \times \frac{2\sqrt{2}\,\pi\,E_0\,\sqrt{E_0}}{n^2\,m\,\sqrt{m}\,\Delta_\perp^2} \cdot e^{aE_0} \cdot erfc(\sqrt{aE_0}) \tag{71}$$

It shall be noted that this formula involves the multiplication of a very small number with a very large one:

$$erfc(\sqrt{aE_0}) \sim e^{-374} \quad e^{aE_0} \sim e^{+370} \tag{72}$$

Therefore, to perform the numerical computations in this paper the Mathematica software was used requiring a precision of 40 digits. Alternatively, serie expansions can be used for these functions ([3] 7.1.2.8), provided that terms of the same order are multipied together before performing the summation.

REFERENCES

1. Bethe, Salpeter,"Quantum Mechanics of one and two electrons systems", Encyclopedia of Physics edited by S. Flügge Volume XXXV Atom I, Springer 1957.
2. R. Neumann, H. Poth, A. Winnacker, A. Wolf, Z. Phys. A - Atoms and Nuclei 313, 253-262 (1983)
3. M. Abramowitz, I.A. Stegun, "Handbook of Mathematical Functions"
4. F.B. Youssif, P. Van de Donk, Z. Kucherovsky, J. Reis, E. Brannen, J.B.A. Mitchell, Phys. Rev, Lett. 67, 26-29 (1991)
5. U. Schramm, J. Berger, M. Grieser, D. Habs, E. Jaeschke, G. Kilgus, D. Schwalm, A. Wolf, Phys. Rev, Lett. 67, 22-25 (1991)
6. L. Vàlyi, "Atom and Ions sources", ISBN 0 471 99463 4, (1977)
7. G.I. Budker, N.S. Dikanski, V.I. Kudelainen, I.N.Meshkov, V.V. Parchomchuk, D.V. Prestikov, A.N. Skrinski, B.N. Sukhina, Part. Accel. 7, 197 (1976) and Studies on electron cooling of heavy particle beams, CERN 77-08 (1977).
8. A. Bachelier, E. Luc-Koenig, J. Phys. B 13,1743 and 1769, (1980).
9. V. D. Kondratovich, V. N. Ostrovsky, J. Phys. B 17, 1981 and 2011, (1984); 23, 3785, (1990).
10. W. L. Glab, M. H. Nayfeh, Phys. Rev. A 31, 530 (1985).
11. H. Rottke, K.H. Welge, Phys. Rev. A 33, 301 (1986).
12. S. R. Lundeen, F. M. Pipkin, Metrologia 22, 9 (1986).
13. C. W. Fabjan, F. M. Pipkin, Proceedings of the International Conference for Precision Measurements and Fundamental Constants, Gaithersburg august 1970, National Bureau of Standards Special Publication No 343, 377 (1971).
14. C. W. Fabjan, F. M. Pipkin, Phys. Lett. 36 A, 69 (1971).
15. C. W. Fabjan, F. M. Pipkin, Phys. Rev. A 6, 556 (1972).
16. F. M. Pipkin, Quantum Electrodynamics, 696-773, edited by T. Kinoshita, World Scientific, Singapore 1990.
17. E. W. Hagley, F. M. Pipkin, Phys. Rev. Lett. 72 Nb 8, 1172 (1994).
18. H. Massey, "Negative Ions", Cambridge University Press (third edition 1976), ISBN 0 521 20775 4.
19. T.M Squires, P. Yesley, G. Gabrielse, Stability of a Charged Particle in a Combined Penning-Ioffe Trap, Phys. Rev. Lett. 86, 5266

(2001).
20. G. Gabrielse et al, First positron cooling of antiprotons, Phys. Lett. B 507, 1 (2001).
21. G. Gabrielse, A. Khabbaz, D. S. Hall, C. Heimann, H. Kalinowsky, W. Jhe, Precision Mass Spectroscopy of the Antiproton and Proton Using Simultaneously Trapped Particles, Phys. Rev. Let. 82 No 16 , 3198-3201 (1999).
22. K. S. Fine et al, The ATHENA antihydrogen experiment, AIP Conf. Proc. : 498 (1999) , pp.40-47.
23. H. C. Bruyant, K. B. Butterfield, D. A. Clark, J. B. Donahue, P. A. M. Gram, M. E. Hamm, R. W. Hamm, W. W. Smith, "Atomic Physics with Relativistic Beams", in Atomic Physics 7 edited by D. Kleppner and F. M. Pipkin, p29-63, Proceedings of the Seventh International Conference on Atomic Physics, MIT (1980).
24. S. Maury, The Antiproton Decelerator (AD), Lear symposium CERN may 15 1999. CERN/PS-50(HP).
25. C. Carli, F. Caspers, Stochastic cooling at the CERN antiproton decelerator, 7th European Particle Accelerator Conference, 26th-30th june 2000, Vienna Austria. CERN/PS 2000-024(AE)
26. D. Möhl, Production of Low-energy Antiprotons, Hyperfine Interactions 109, 33-41 (1997).
27. M. Hori et al, Sub-ppm laser spectroscopy of antiprotonic helium and a CPT-violation limit on the antiprotonic charge and mass, Phys. Rev. Lett. 87, 093401 (2001).
28. Design study of anti-proton accumulation and deceleration ring in the KEK PS complex. By S. Machida, M. Yoshii (KEK, Tsukuba), Y. Mori, N. Tokuda (Tokyo U., INS), Y. Ishi (Mitsubishi Electric, Tokyo). KEK-PREPRINT-95-17, Apr 1995. 3pp. Contributed paper at 1995 Particle Accelerator Conference and International Conference on High-Energy Accelerators, 1 - 5 May, 1995, Dallas, Texas, U.S.A. In *Dallas 1995, PAC* 360-362.
29. Crystalline beams and related issues, Proceedings of the 31st Workshop of the INFN Eloisatron Project, Erice,Italy 12-21 November 1995, editors D. M. Maletic and A. G. Ruggiero, World Scientific, ISBN 981-02-2785-X.
30. P. J. Channell, F. R. Neri, in "Crystalline beams and related issues", p13-31.
31. The physics of crystalline beam, in "Crystalline beams and related issues", p317-347.
32. I. N. Meshkov, A. N. Skrinski, Nucl. Instr. and Meth. A 391,41, (1996).
33. I. N. Meshkov, A. O. Sidorin, Nucl. Instr. and Meth. A 391, 216, (1997).
34. Chi-Yu Hu, D. Caballero, Z. Hlousek, J. Phys. B: At. Mol. Phys. 34, 331-338 (2001)
35. Michael Charlton, Hyperfine Interactions 109, 269278 (1997).
36. J.P. Merrison ,H.Bluhme , M. Charlton , H. Knudsen and M.R. Poulsen, Hyperfine Interactions 109, 313321 (1997).